Dalton Transactions

In-situ analysis of growth rate evolution during molecular layer deposition of ultra-thin polyurea films using aliphatic and aromatic precursors

Journal:	*Dalton Transactions*
Manuscript ID	DT-ART-11-2021-003689.R1
Article Type:	Paper
Date Submitted by the Author:	12-Dec-2021
Complete List of Authors:	Nye, Rachel; North Carolina State University, Chemical and Biomolecular Engineering Wang, Siyao; North Carolina State University, Chemical and Biomolecular Engineering Uhlenbrock, Stefan; Micron Technology Inc, Technology Development Smythe III, John; Micron Technology Inc, Technology Development Parsons, Gregory; North Carolina State University, Chemical and Biomolecular Engineering

SCHOLARONE™
Manuscripts

ARTICLE

In-situ analysis of growth rate evolution during molecular layer deposition of ultra-thin polyurea films using aliphatic and aromatic precursors

Received 00th October 2021,
Accepted 00th January 20xx

DOI: 10.1039/x0xx00000x

Rachel A. Nye, [a] Siyao Wang, [a] Stefan Uhlenbrock,[b] John Smythe,[b] and Gregory N. Parsons *[a]

Organic thin films formed by molecular layer deposition (MLD) are important for next-generation electronics, energy storage, photoresists, protective barriers and other applications. This study uses in situ ellipsometry and quartz crystal microbalance to explore growth initiation and growth rate evolution during MLD of polyurea using aromatic p-phenylene diisocyanate (PDIC) or aliphatic 1,6-hexamethylene diisocyanate (HDIC) combined with ethylenediamine (ED) or 1,6-hexanediamine (HD) co-reactants. During the first 10-20 cycles of growth, we show the growth rate can increase and/or decrease substantially depending on the substrate as well as the flexibility, length, and structure of the isocyanate and amine reactants used. The transition from initial to steady growth is attributed to a change in active surface site density as the growth proceeds, where the number of sites is determined by a balance between steric effects that block active sites, double reactions that consume multiple active sites, and precursor physisorption and sub-surface diffusion that create new active sites, where the extent of each mechanism depends on the precursors and deposition conditions. Results shown here provide useful insight into mechanisms needed to control growth of ultra-thin organic films for advanced applications.

Introduction

Molecular layer deposition (MLD) has drawn increasing interest for its potential to precisely tune the structure and functionality of organic or hybrid organic/inorganic thin films for applications in microelectronics,[1,2] battery electrodes,[3] catalysts,[4] solar cells,[5] capacitors,[6,7] and biomedical devices.[8] Analogous to atomic layer deposition (ALD), MLD is a low temperature (typically < 200 °C) processing technique that utilizes sequential, self-limiting vapor-solid surface reactions to build up conformal organic polymer, oligomer, or metal coordination (i.e. metal-organic or organic/inorganic) thin films on receptive surfaces.[9,10] The saturated self-limiting reactions enable highly controllable thickness and conformality at the molecular level. Furthermore, film properties including electrical[11,12] and thermal[13] conductivity, mechanical durability,[14,15] and magnetic properties[16,17] may be tuned by varying monomer structure or deposition temperature. This tunability has recently been exploited to create photoresists,[18,19] coat batteries and catalysts,[20] and form metal-organic network or metal-organic framework materials.[21–25] Thus, understanding the MLD film growth mechanism with different precursors is essential for film property control and ultimately film application in various fields.

[a.] Department of Chemical and Biomolecular Engineering, North Carolina State University, 911 Partners Way, Raleigh, North Carolina 27606
Email: gnp@ncsu.edu
[b.] Micron Technology Inc, 8000 S Federal Way, Boise, Idaho 83716
Electronic Supplementary Information (ESI) available: FTIR of polyurea HDIC/ED films deposited between 5-50 nm thick at 60 °C. See DOI: 10.1039/x0xx00000x

MLD is commonly conducted with two homo-bifunctional precursors,[20] although MLD using multi-functional precursors[26] or combinations of three-precursors[27] has also been demonstrated. In ideal MLD with homo-bifunctional precursors, one end of the molecule reacts and consumes a single reactive surface site, so that the other end becomes a new site available to react during the next reactant dose. In some cases, it is also possible for both ends of the precursor to react and consume two reactive sites, i.e. via a “double reaction” (DR), which creates no new reactive sites.[28–30] Another possibility is that a precursor may adsorb onto the growing surface or absorb via diffusion into the growing film.[28] Precursor adsorption/absorption does not consume reactive surface sites, but does generate new sites available for the next precursor dose. Accordingly, monomer adsorption on or diffusion into the polymer surface is expected to play an important role in MLD growth.[31,32]

During MLD, the rate of site consumption (by DR’s) and site generation (by adsorption/diffusion) will depend on process conditions, deposition reactants, and importantly, the amount of film deposited. For example, the extent of reactant adsorption on the starting growth substrate (e.g., SiO_2) will likely be different from that on the growing polymer/hybrid film. The extent of sub-surface diffusion will also depend on the amount of film present.[32,33] As growth proceeds, the rate of site consumption and diffusion/adsorption will become constant, resulting in a constant growth rate in a steady growth regime.[34] The transition from initial to steady growth will depend on deposition temperature, composition and reactivity of the growth surface, and precursors used. For example, longer, more flexible monomers are expected to undergo DRs more readily,

as these flexible chains can bend more easily. The increased frequency of DR site terminations thereby leads to an observed smaller steady growth rate compared to films incorporating shorter, stiffer monomers.[35]

Polyurea, with its chemical and moisture resistant properties,[36] can be formed via MLD using diamine and diisocyanate precursors under a wide range of deposition temperatures (room temperature (RT) to 90 °C). Several options for diamine precursors include ethylenediamine (ED),[37] 1,6-hexanediamine (HD),[34] 1,4-diaminobutane,[38] and p-phenylenediamine.[39] However, the diisocyanate reactant is typically limited to p-phenylene diisocyanate (PDIC) for polyurea[20,35] and polyurethane[40] MLD. PDIC is not an ideal precursor because it is a solid at RT (melting point ~97.5 °C) with a low vapor pressure (<0.01 mmHg at 20 °C), so that valves and gas delivery lines require careful temperature control to avoid condensation.[41] Furthermore, the thermal stability of PDIC is not well known. Polyurea MLD has been reported using 1,4-diisocyanatobutane,[35] but the high cost (~100 x more than PDIC) makes it less attractive.

In this work, we explore MLD of polyurea using PDIC as well as 1,6-hexamethylene diisocyanate (HDIC) as a novel MLD precursor. HDIC is liquid at RT (vapor pressure = 0.05 mmHg) with a similar cost to PDIC. We analyze the thermal stability of PDIC and HDIC and show that HDIC can be delivered at lower temperature (55 °C) and has favorable stability during prolonged heating (>10 months). We also compare MLD using PDIC and HDIC with various diamine reactants and show successful growth with the novel precursor.

Finally, we discuss new insights from the high flexibility of the six-carbon HDIC monomer on site generation and termination during MLD. Previous work has analyzed flexibility related trends in polymer chain orientation, crystallinity, packing density, and strength of intermolecular forces.[35] We expand this knowledge by systematically studying the initial and steady growth rates for a range of monomers with different flexibilities, in particular with in situ ellipsometry measurements for increased understanding of growth transitions. Furthermore, we describe the observed nonlinear growth with a simple growth rate transition model based on monomer structure and deposition temperature. This insight is critical for reliable deposition of ultra-thin MLD films in advancing technologies.

Experimental

Materials

The precursors ED, HDIC (Acros Organics), PDIC, and HD (Sigma Aldrich) were used as received. All materials were transferred into glass ampoules in a nitrogen-purged glovebox before being installed onto the MLD reactor. Typical substrates were boron-doped silicon (100) wafers (5-10 Ω-cm resistivity) that were cleaned in piranha solution of 1:1 volume ratio H_2O_2:H_2SO_4 for 15 minutes before use. These substrates had a ~2 nm chemical oxide layer measured by spectroscopic ellipsometry (SE), which are referred to herein as hydroxylated SiO_2.

Reactor and Deposition Conditions

Deposition was conducted in a home-built, warm-walled, viscous-flow MLD reactor consisting of a 12-inch diameter spherical chamber equipped with several additional ports for in situ analysis. Fig. 1 shows a schematic of the reactor including precursor delivery lines, which were described previously.[34] The chamber incorporates an in situ ellipsometer (ISE) at an incidence angle of ~65°, with pneumatically operated gate valves to prevent deposition on the fused silica viewports. These valves are controlled by LabVIEW software to open simultaneously during purging to conduct measurements.

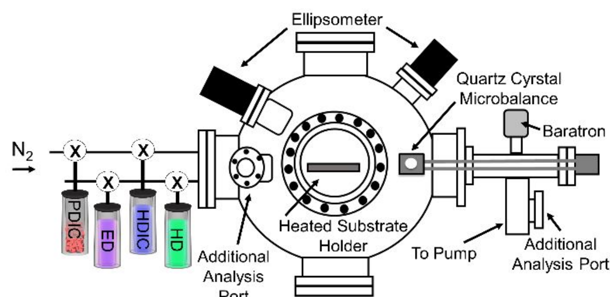

Fig. 1 Schematic of MLD reactor incorporating in situ analytical tools of ellipsometry and QCM, with additional ports for future analysis (e.g. FTIR and QMS).

The chamber includes a cylindrical extension (~1.5-inch inner diameter and ~5 inches in length) to house a quartz crystal microbalance (QCM) probe, which enables simultaneous measurements from QCM (on a QCM crystal) and ellipsometry (on a Si wafer). A heated substrate holder in the center of the spherical chamber heats the substrates quickly and uniformly using three 500 W resistive heating cartridges (Omega) controlled by Variac variable transformers. The QCM probe is located next to (but not in contact with) this heated substrate holder, and is heated convectively from the chamber walls and substrate holder. The substrate holder and QCM probe are monitored with thermocouples to verify consistent temperatures during deposition. The reactor features additional ports to accommodate other supplementary analytical instruments in the future, such as Fourier transform infrared (FTIR) spectroscopy and quadrupole mass spectrometry (QMS). Pure nitrogen (N_2, 99.999%, Arc3 Gases) serves as the carrier and purge gas, which passes through an Entegris Gatekeeper for additional purification before entering the chamber.

Individual precursors are heated as follows to achieve sufficient vapor pressure during deposition: PDIC (60 °C), HDIC (60 °C), HD (50 °C), and ED (RT). For thermal stability analysis, the effects of additional temperatures of 110 °C for PDIC and 55 °C for HDIC were also evaluated. The typical operating pressure is 400 mTorr, achieved with 90 standard cubic centimeters per minute (sccm) of N_2 flow. Typical operating temperatures range from 30-100 °C.

The precursor exposure cycle typically includes a reactor pump-down step followed by a reactant pulse and a pressure-hold (i.e. "soak") step, where the pulse and soak steps are

This journal is © The Royal Society of Chemistry 20xx

performed with no N_2 flow and the pump valves closed. The total dose time includes the pulse and soak times. The typical pump-down/pulse times for PDIC, HDIC, HD, and ED are (60 s/20 s), (30 s/10 s), (30 s/5 s), and (20 s/1.2 s), respectively. The pump-down step allows the reactor pressure to be < 100 mTorr. The reactant soak step is 30-60 s. The reaction half-cycle is then completed by performing a N_2 purge step for 30-60 s. All depositions in this study are performed following this sequence with specific times specified unless stated otherwise.

For some QCM experiments, the gold-coated QCM crystal was pre-coated with 50 ALD cycles (~5 nm) of Al_2O_3 from trimethylaluminum (TMA) and deionized water (DI H_2O). This film was deposited at 90 °C and 400 mTorr using a deposition sequence of (TMA pulse/N_2 purge/H_2O pulse/N_2 purge) with the following times: (0.1 s/60 s/ 0.1 s/60 s).

Characterization

Film thickness and refractive index were measured with ex situ and in situ ellipsometry. The ex situ measurements were performed with a J. A. Woollam Co. alpha-SE spectroscopic ellipsometer at an incidence angle of 70 ° relative to the surface normal and a spectral range of 300-900 nm. In situ measurements were performed with a Film Sense FS-1 multiwavelength ellipsometer, which recorded thickness and optical values at wavelengths of 436, 521, 599, and 638 nm. In situ measurements taken every cycle determined the instantaneous growth rate of MLD films. Both ellipsometers used Cauchy models available with the software packages, which were verified with scanning electron microscopy (SEM) and x-ray reflectivity (XRR) thickness values. Each sample measured by ex situ ellipsometry was measured at three different locations to ensure uniformity, with the average value compared to in situ measurements. All thicknesses reported here are the result of in situ ellipsometry measurements unless stated otherwise. Uncertainty in film thickness is generally ± a few percent.

QCM was used to measure mass uptake during deposition. This was performed with a Kurt Lesker probe body and Inficon gold-coated crystal sensor. A N_2 purge on the backside of the crystal was used to prevent coating of electrical components. Data was collected using an STM2 control box (Inficon). Additional characterization of film composition was conducted with FTIR using a Thermo Scientific Nicolet 6700 spectrometer with a dry air purge and a DTGS KBr detector. Each spectra was collected using 200 scans at 4 cm^{-1} resolution with 64 scans of hydroxylated SiO_2 as the background.

Characterization of the PDIC precursor decomposition was performed at Micron Technology Inc. Attenuated total reflectance (ATR) FTIR was performed on powder samples with 250 co-added scans on a Harrick GATR accessory (Ge crystal) on a Thermo Nicolet 8700 bench with a range of 650-4000 cm^{-1} and 4 cm^{-1} resolution using a DTGS KBr detector. Melting point of the PDIC samples was taken with an Electrothermal 9100 instrument by heating a small amount of sample in a glass capillary tube at 0.2 °C/min and visually determining when the sample converted from solid to liquid. CHN combustion analysis was performed on an Exeter Analytical CE-440 with 1.5 mg of sample encapsulated in sealed tin vessels. The carbon, hydrogen, and nitrogen concentrations were measured with a series of thermal conductivity cells by combusting at 980 °C, reducing at 650 °C, and filtering the samples. Reported values are the average of triplicate analysis. The remainder mass percent of each sample is considered to be primarily oxygen. Direct insertion probe mass spectrometry (DIP-MS) was performed on a Thermo ISQ LT single quadrupole mass spectrometer with direct insertion probe, a scan range of 40 to 1100 m/z, and 0.5 amu resolution.

Results

Thermal Stability of Diisocyanate Precursors

The chemical structure of the diisocyanate and diamine precursors used in this study are shown in Fig. 2. We study the stability of diisocyanate precursors (PDIC and HDIC) because their vapor pressures are small compared to the diamine reactants, so for use in manufacturing, the PDIC and HDIC must be maintained at relatively high temperatures for prolonged periods. PDIC and HDIC are referred to here as "aromatic" and "aliphatic," respectively. Similarly, ED and HD may be referred to as "2C" (i.e., 2-carbon chain) and "6C" (i.e., 6-carbon chain), respectively. For MLD studies, the as-received reactants are placed in a dry glove box where they are transferred into glass delivery vessels and back-filled with N_2. On the MLD reactor, the precursor vessels are heated to 110, 55, 50 °C and RT for PDIC, HDIC, HD, and ED, respectively, which are above the melting points of 96-99 °C,[42] -67 °C,[43] 42 °C,[44] and 8 °C,[45] respectively. For the first several months of operation, these heating conditions result in reproducible MLD. However, after ~6 months, the growth rate of the PDIC/ED becomes slower and inconsistent, which is ascribed to thermal degradation of PDIC. In contrast, extended studies of HDIC/ED show consistent growth over more than ten months.

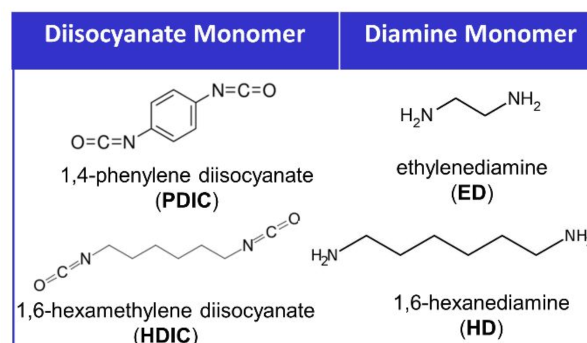

Fig. 2 Chemical structures of the diisocyanate and diamine precursors used in this study.

Please do not adjust margins

Table 1 Heating conditions and corresponding visual, melting point, and CHN combustion analysis results for PDIC and HDIC precursors under inert ambient in vessels on the MLD reactor

Material	Condition	Color	Melting Point (°C)	C (wt.%)	H (wt.%)	N (wt.%)	Remainder (wt.%)
PDIC	Expected	White/yellow	96-99	60.00	2.52	17.50	19.98
	As Received	White	95	58.84	2.30	17.01	21.86
	6 months at 110 °C	Brown	>130	59.98	2.27	17.43	20.31
	12 months at 60 °C	Yellow/brown	>130				
HDIC	Expected	Clear/pale yellow liquid	-67				
	As Received	Clear liquid					
	10 months at 55 °C	Clear liquid					

To understand the long-term stability trends in deposition of PDIC/ED vs HDIC/ED, we evaluate the composition and bonding of the PDIC and HDIC precursors in the as received state and after extended heating. Materials are characterized by melting point measurement and combustion analysis (to determine atomic percent of C, H, and N) before and after heating, and results are given in Table 1. The bonding structure is determined by direct insertion probe mass spectrometry (DIP-MS), with results given in Fig. 3.

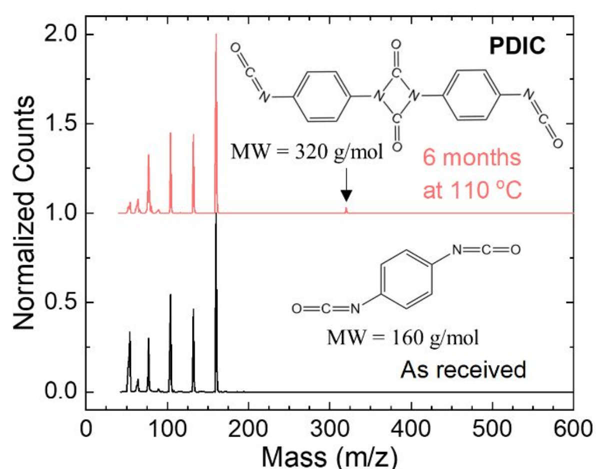

Fig. 3 DIP-MS spectra of PDIC as received (black) and after heating at 110 °C for six months (red).

Consider first the melting point temperatures. As received, the PDIC is a fine white solid powder which melts at ~95 °C. After extended heating at 110 °C the PDIC is removed from the reactor, cooled to room temperature, and is observed to be a brown-colored powder. Upon reheating, this sample remains solid up to 130 °C. Combustion analysis of carbon, hydrogen, and nitrogen (Table 1) shows that the PDIC composition is approximately the same before and after heating.

The results of DIP-MS analysis (Fig. 3) for the as received PDIC sample demonstrate strong peaks at 160 amu ($C_8H_4N_2O_2$, PDIC) as well as at 77, 104, and 132 amu corresponding to fragments of PDIC, namely C_6H_5, $C_6H_4N_2$, and $C_7H_4N_2O$, respectively. No compounds above the molecular weight of the PDIC monomer are detected. However, the PDIC sample heated to 110 °C for six months exhibits a peak at 320 amu, corresponding to the dimerized form of PDIC. The PDIC trimer (480 amu) is not observed in this analysis.

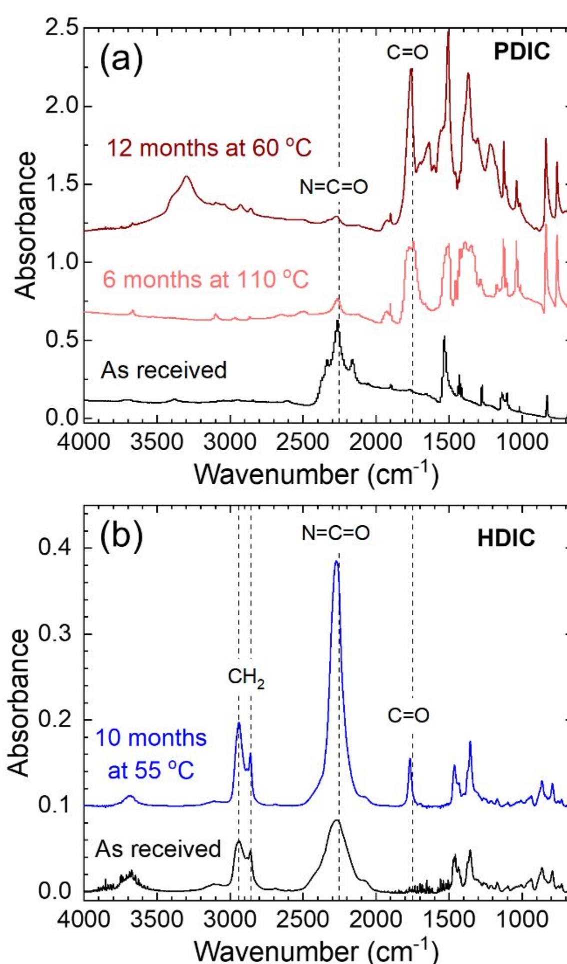

Fig. 4 FTIR spectra of as received (black) and heated diisocyanate precursors: (a) PDIC at 60 °C for twelve months (dark red, top) and at 110 °C for six months (light red, middle), and (b) HDIC at 55 °C for ten months (blue).

FTIR results for the two diisocyanate monomers before and after heating are shown in Fig. 4. The spectra for each as received sample display a prominent N=C=O isocyanate peak at 2250 cm^{-1}.[2] The heated PDIC samples have much weaker isocyanate peaks, and instead demonstrate strong C=O peaks at

This journal is © The Royal Society of Chemistry 20xx

1700 cm^{-1}.[2] It is notable that almost complete conversion of isocyanate to carbonyl is observed for PDIC even when heated below the melting point (i.e. 60 °C). Additional peaks for the heated PDIC samples are observed at 1370 cm^{-1} and 3290 cm^{-1}, attributed to C-N stretching and N-H stretching, respectively.[35] For the heated HDIC sample, the C=O peak at ~1700 cm^{-1} is also observed. However, in this case, the carbonyl peak is small relative to the strong isocyanate peak at 2250 cm^{-1}.

The unchanged chemical composition and increased melting point of PDIC after heating (Table 1) are consistent with monomer self-polymerization.[46–48] This mechanism is supported by conversion of isocyanate (C=N=O) groups to carbonyl (C=O) groups and the increased C-N stretching observed by FTIR in Fig. 4a for heated PDIC. The additional N-H peak present in the heated PDIC sample suggests the presence of additional organic byproducts consistent with decomposition of an amino-compound. Presence of the dimer but not the trimer in DIP-MS analysis (Fig. 3) indicates dimerization is the extent of PDIC self-reaction under conditions used here. Although dimerization of HDIC is also known to occur,[49] FTIR results (Fig. 4b) indicate that HDIC remains predominantly in the monomer form after heating under the conditions specified in Table 1. These results confirm that the thermal decomposition of HDIC proceeds much more slowly than for PDIC under MLD conditions, making this a promising candidate for further study.

MLD Reaction Saturation

We next work to explore reaction saturation for various combinations of polyurea precursors. Generally, MLD processes are not fully saturated due to non-self-limiting physisorption reactions, creating a so-called "soft" saturation.[28,34,50] The PDIC/ED and PDIC/HD processes were explored previously with ex situ ellipsometry measurements.[34] For each process the total pulse time of one precursor was maintained constant while the other was varied between 0-60 s (PDIC), 0-3 s (ED), and 0-10 s (HD) for twenty MLD cycles deposited at 60 °C on SiO_2. A ten second soak time was used after each precursor pulse. The required pulse times for soft saturation were 30 s, 1 s, and 5 s for PDIC, ED, and HD, respectively.

Reaction saturation for the HDIC/ED process is studied using in situ ellipsometry, where the growth rate is extracted from half-cycle measurements so that saturation can be determined in a single deposition run.[51] Results are shown in Fig. 5. As described in the Experimental section, the HDIC and ED dose sequences involved pump/pulse/soak/purge steps. In each case, ten cycles of polyurea were deposited at 40 °C on SiO_2.

To evaluate the HDIC saturation, the HDIC and ED pump/pulse/soak/purge sequence step times were set at 60/3/30/60 s and 20/1.5/30/90 s, respectively. Each deposition cycle consisted of five HDIC dose sequences followed by one ED dose sequence. Using the in-situ ellipsometer, the thickness is measured during each purge step (i.e. 6 times per cycle). Data is collected over the 10 full cycles, and results are shown in Figure 5a. As discussed in a following section, Fig. 5a shows that on SiO_2, the growth rate changes during the initial cycles,[34] with the largest change during the first ~5 cycles. To evaluate saturation after growth initiation, Fig. 5c is a plot of thickness change per HDIC/ED cycle where each data point in the plot corresponds to the average accumulated thickness change measured after each HDIC dose sequence during cycles 6-10 in Fig. 5a. The error bars correspond to the standard deviation of the measured values. From Fig. 5c, saturated thickness change is ~0.058 $\pm$ 0.004 nm/cycle, which is achieved after 12 s HDIC pulsing.

Similarly, ED saturation is evaluated using one HDIC sequence with pump/pulse/soak/purge = 60/12/30/60 s followed by five ED sequences with pump/pulse/soak/purge = 20/0.3/30/90 s. As with HDIC, the thickness change was measured 6 times per cycle, and the complete data set is shown in Figure 5b. Likewise, the average thickness per cycle is plotted in Figure 5d. After ~1.2 s total ED pulse time, the thickness change is ~0.052 $\pm$ 0.006 nm/cycle, consistent with the value from Fig. 5c. The results show reasonable reaction saturation, with evidence for some continued growth (i.e. soft saturation associated with reactant physisorption) consistent with other MLD reactions.[28,34,50] For the experiments below, unless otherwise noted, the HDIC and ED pump/pulse/soak/purge sequence times were set at 60/10/30/60 and 60/1.2/30/60 s, respectively.

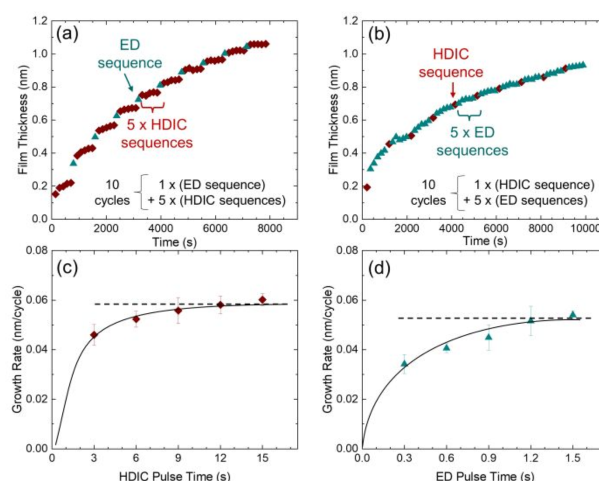

Fig. 5 Thickness measured by in situ ellipsometry as a function of time for 10 cycles HDIC/ED deposited at 40 °C on hydroxylated SiO_2 with (a) five repeated HDIC dose sequences and (b) five repeated ED dose sequences. Each dose consists of (pump/pulse/soak/purge) for HDIC (red diamonds) and ED (green triangles). (c) Average growth rate (nm/cycle) per HDIC/ED cycle as a function of HDIC pulse time, obtained by averaging the data from cycles 6-10 in panel (a). (d) Average growth rate per HDIC/ED cycle as a function ED pulse time from the data in cycles 6-10 in panel (b). Lines are drawn as guides to the eye.

Polyurea Composition

A comparison between film compositions for the four different polymers is performed with FTIR for thick polymer samples (>10 nm) deposited using saturated conditions. Spectra are shown in Fig. 6. The characteristic urea linkages of amide I (attributed primarily to the C=O stretch at 1600-1700 cm^{-1}) and amide II (including contributions from C-N stretching and N-H bending) are observed at ~1640 cm^{-1} and ~1545 cm^{-1}, respectively.[2,35] A broad N-H stretch at 3250-3400 cm^{-1} and an N-C-N stretch at ~1250 cm^{-1} are also apparent for all films.[52] The aromatic ring modes at ~1500 and 1400 cm^{-1} are apparent only for the aromatic PDIC/ED and PDIC/HD films.[37] The CH_2 stretch around 2850 – 2950 cm^{-1} is the strongest for the aliphatic HDIC/ED and HDIC/HD films.[37] The PDIC/ED sample does not have enough CH_2 groups present at this thickness for this peak to be detected. The N=C=O isocyanate stretch at 2270 cm^{-1} is not observed in any of the films, consistent with nearly complete reaction between the diisocyanate and diamine precursors.[2]

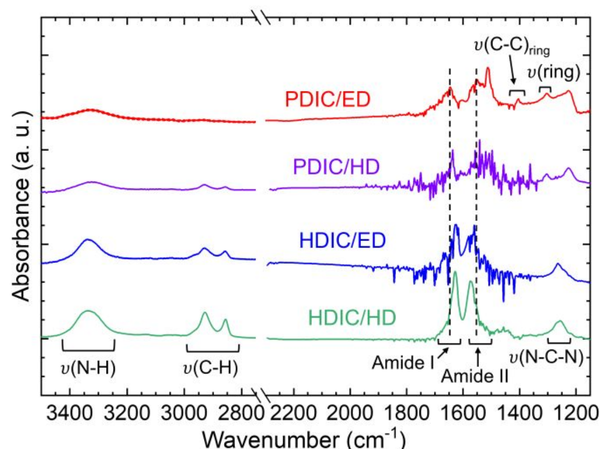

Fig. 6 FTIR spectra of >10 nm thick aromatic PDIC/ED (red), PDIC/HD (purple), and aliphatic HDIC/ED (blue), and HDIC/HD (green) films, demonstrating characteristic urea linkages. Vertical dashed lines are guides to the eye. In the aliphatic films, the amide I and amide II peaks show decreased peak-splitting relative to the aromatic films.

In the aliphatic films, the amide I and amide II peaks show significant red- and blue-shifting, respectively, relative to the aromatic films.[35] This shifting and the intensifying of the peaks have been previously observed in polyurea films,[35,53] and is attributed to hydrogen-bonding (e.g. between the amide N-H groups and an adjacent carbonyl oxygen) between adjacent chains causing a variety of bond lengths and strengths throughout the film.[54,55] Further investigation on the shifting of these peaks was conducted for different thicknesses of HDIC/ED films between 5-50 nm thick (Supporting Fig. 1), with no significant difference in peak location observed over this thickness range.

Polyurea Growth Evolution

Backbone Flexibility and Temperature Effects on Growth. Polyurea growth evolution is compared between polymers using in situ ellipsometry and QCM. One hundred cycles of each polyurea film are deposited at 60 °C on hydroxylated SiO_2 using saturated conditions. Thickness is measured every cycle using in situ ellipsometry (PDIC/HD is deposited at 45 °C and measured every cycle for the first twelve cycles, then measured every ten cycles to cycle 100), with results shown in Fig. 7. The structure of one unit group for each polymer is shown in Fig. 7a. Fig. 7b and c show thickness and growth per cycle, respectively, as a function of cycle on SiO_2. For each polymer, growth proceeds rapidly on SiO_2 and gradually slows down over the first ~20 cycles.[34,35] After ~20 cycles, growth proceeds linearly at a rate of 0.32, 0.13, 0.014, and 0.020 nm/cycle for PDIC/ED, PDIC/HD, HDIC/ED, and HDIC/HD, respectively. Growth rate generally decreases with increasing backbone flexibility.[34,35] The initial and linear growth rates of the two most flexible backbones (aliphatic films) are similar, although slightly larger for the longer aliphatic film (HDIC/HD). The relatively higher noise for the PDIC/ED data could be due to the relatively higher thickness of these films at a given cycle number, which may cause some inaccuracies in ellipsometry measurements when using the same measurement parameters as for the thinner films.

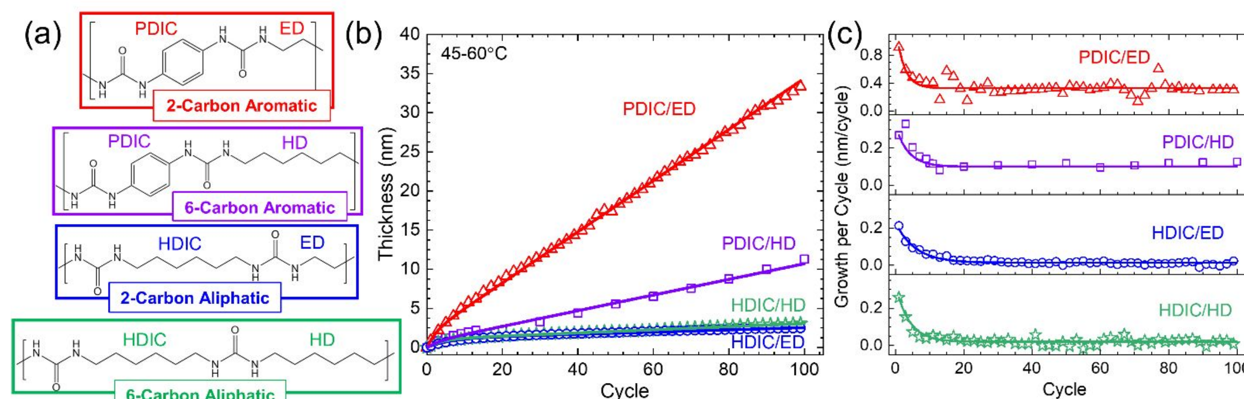

Fig. 7 (a) Polymer structures and (b) thickness and (c) growth rate as a function of MLD cycle, determined from in situ ellipsometry for PDIC/ED (red triangles), PDIC/HD (purple squares), HDIC/ED (blue circles), and HDIC/HD (green stars) for deposition on hydroxylated SiO_2 at 60°C. Lines in (b) and (c) correspond to model fits discussed later and presented in Table 2. Experimental data points are only included on odd cycle numbers for clarity.

 This journal is © The Royal Society of Chemistry 20xx

A representative aromatic (PDIC/ED) and aliphatic (HDIC/ED) film are further investigated with QCM measurements shown in Fig. 8. The same diamine reactant is used in each film to focus the comparison on the diisocyanate precursors. For this experiment, films are deposited on gold QCM crystals pre-treated with aliphatic polyurea. The 2C-aromatic film has a much higher mass growth rate than the 2C-aliphatic film, consistent with ellipsometry results (Fig. 7). Fig. 8b shows the mass uptake for each individual precursor during steady growth, taken from the boxed regions of Fig. 8a. For both polymers, the diisocyanate doses result in higher mass uptake, consistent with their higher molecular weights compared to the diamine precursors. The additional mass uptake during the pump-down step in the HDIC/ED process is attributed to precursors desorbing from the chamber walls, some of which adsorb/react on the QCM crystal. The average mass uptake per cycle is ~36 ng/(cm^2 cycle) for 2C-aromatic films and ~6 ng/(cm^2 cycle) for 2C-aliphatic films. This equates to a thickness gain of 0.28 and 0.052 nm/cycle at 60 °C for the aromatic and aliphatic films, using densities of 1.3 and 1.15 g/cm^3 determined by XRR, respectively. These values are reasonably close to the growth rates measured by ellipsometry in Fig. 7.

The temperature dependence of aliphatic film growth is explored by depositing 100 cycles of 2C- and 6C-polyurea on SiO_2 between 30 and 100 °C. Corresponding in situ ellipsometry results are shown in Fig. 9. Growth rate generally decreases with increasing temperature, consistent with previous reports of polyurea deposited from aromatic PDIC between 45 – 90 °C.[34] This is attributed to monomer dissociation from the growth surface at higher temperatures.[56,57] While the 2C-aliphatic film still deposits slowly at 100 °C (Fig. 9a), the 6C-aliphatic film does not have significant growth at temperatures ≥ 80 °C (Fig. 9b). Both films are successfully deposited as low as 30 °C, making them suitable candidates for low-temperature applications.

Observational Kinetic Modeling. The results above demonstrate a strong dependence of growth rate on cycle number for the first ~20 cycles. We thus seek to predict growth rate as a function of cycle based on the observed initial and steady growth rates under a given set of deposition conditions (e.g. fixed temperature and starting substrate). We hypothesize that the growth trends can be described by two parallel, first-order elementary reactions with corresponding rate constants k_0 and $k_1(n)$, where $k_1(n)$ is dependent on cycle number, n. Then, we define $k_1(n)$ as:

$$k_1(n) = k_\infty(1 - e^{(-n/\gamma)}) \quad (1)$$

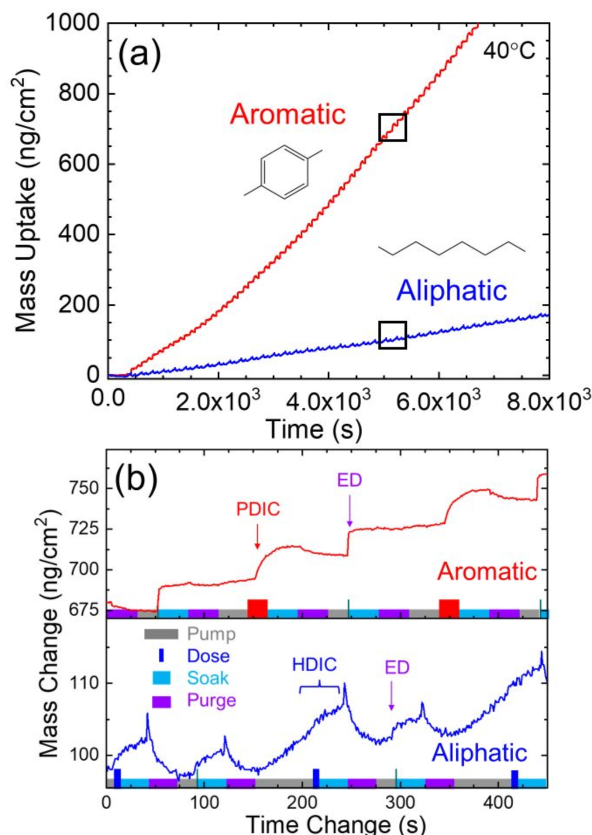

Fig. 8 QCM data for 2C-aromatic (red) and 2C-aliphatic (blue) films, showing (a) mass uptake versus time at 60 °C and (b) enlargement of the boxed region from (a), showing mass uptake for individual monomer doses.

where the transition parameter γ is the characteristic number of cycles at which the transition in growth rate occurs. This definition allows k_1 = 0 at n = 0 (i.e. initial growth depends only on k_0), and k_1 = k_∞ at n >>0 (i.e. the rate becomes constant after many cycles). The overall rate constant is $k(n) = k_0 + k_1(n)$. Expressing the growth rates in terms of the rate constants: $\dot{G}(n) \propto k(n)$, $\dot{G}_0 \propto k_0$, and $\dot{G}_\infty \propto k_\infty$, we obtain:

$$\dot{G}(n) = \dot{G}_\infty + (\dot{G}_0 - \dot{G}_\infty)e^{(-n/\gamma)} \quad (2)$$

where $\dot{G}_0$ and $\dot{G}_\infty$ are the initial and steady growth per cycle, respectively. The values for $\dot{G}_0$ and $\dot{G}_\infty$ can be obtained directly from the experimental trends, and the value for γ is adjusted to obtain the best fit by minimizing the residue sum of squares. The film thickness is acquired by integrating the GPC over a fixed

cycle number. Corresponding fitting parameters are summarized in Table 2. Model fits to thickness data presented in this work are included as solid lines in Fig. 7b-c and Fig. 9a-b, demonstrating good agreement between modelled and experimental thicknesses while maintaining consistent values for $\dot{G}_\infty$ and $\dot{G}_0$.

Previous modelling efforts typically hypothesize reaction schemes and then incorporate or estimate numerous kinetic and thermodynamic properties, such as relevant rate constants, activation energies, sticking coefficients, etc.[28,57,58] In contrast, our analysis does not require significant prior knowledge of the process, and we do not assign specific molecular mechanisms to the parallel reactions. Instead, we use data fits to observe trends in the γ parameter to gain insight into possible mechanisms, examined in the Discussion Section. This information, obtained from a single fitting parameter, is integral to using MLD films in advance applications, for example in area selective deposition.[58–61]

Fig. 9c summarizes the initial (<25 cycles) and steady growth rates for each film as a function of temperature. Initial growth rate decreases significantly with increasing temperature. Steady growth rates also decrease with increasing temperature, but to a much smaller extent. The difference in temperature dependence between initial and steady growth is presented in the Discussion section in terms of monomer diffusion, adsorption, and desorption on metal oxide substrates versus deposited polymer surfaces.

Substrate Effects on Growth. To better understand the effect of the starting substrate surface on initial growth and growth evolution, polyurea growth is also evaluated on metal oxide, aliphatic (HDIC/ED), and aromatic (PDIC/ED) polymer substrates using in situ ellipsometry and QCM. For in-situ ellipsometry, metal oxide substrates are hydroxylated SiO_2. The aromatic and aliphatic substrates are hydroxylated SiO_2 pre-coated with 30 cycles of PDIC/ED or HDIC/ED, respectively. For QCM, the metal oxide substrates are QCM crystals pre-coated with ~5 nm ALD Al_2O_3. The aromatic and aliphatic substrates are prepared in the same way as for ellipsometry measurements, i.e., by pre-coating the substrate (QCM crystals in this case) with 30 cycles of PDIC/ED or HDIC/ED, respectively.

The metal oxide and polyurea substrates are then each coated with two types of polyurea, creating four sample sets: a) aliphatic polyurea (HDIC/ED) on metal oxide; b) aromatic (PDIC/ED) on metal oxide; c) aliphatic on aromatic; and d) aromatic on aliphatic. Each deposition is performed for 40 cycles at 60 °C. In each run, the QCM and ellipsometry data are collected simultaneously, and the results are shown in Fig. 10. For the aromatic growth in Fig. 10b, each GPC value is the average over three cycles.

For growth on metal oxide (Fig. 10a-b), the growth rate for both the aliphatic and aromatic films is fast for the first several cycles, then decreases to a near constant rate after ~20 cycles. On the aromatic substrate (Fig. 10c), the aliphatic deposition rate follows a similar trend. However, on the aliphatic substrate, the aromatic growth shows a markedly different trend. During the first ~20 cycles, the rate initially increases to a maximum then decreases to a near steady value. The differences in polymer growth rates on different polymer substrates are examined in the Discussion section.

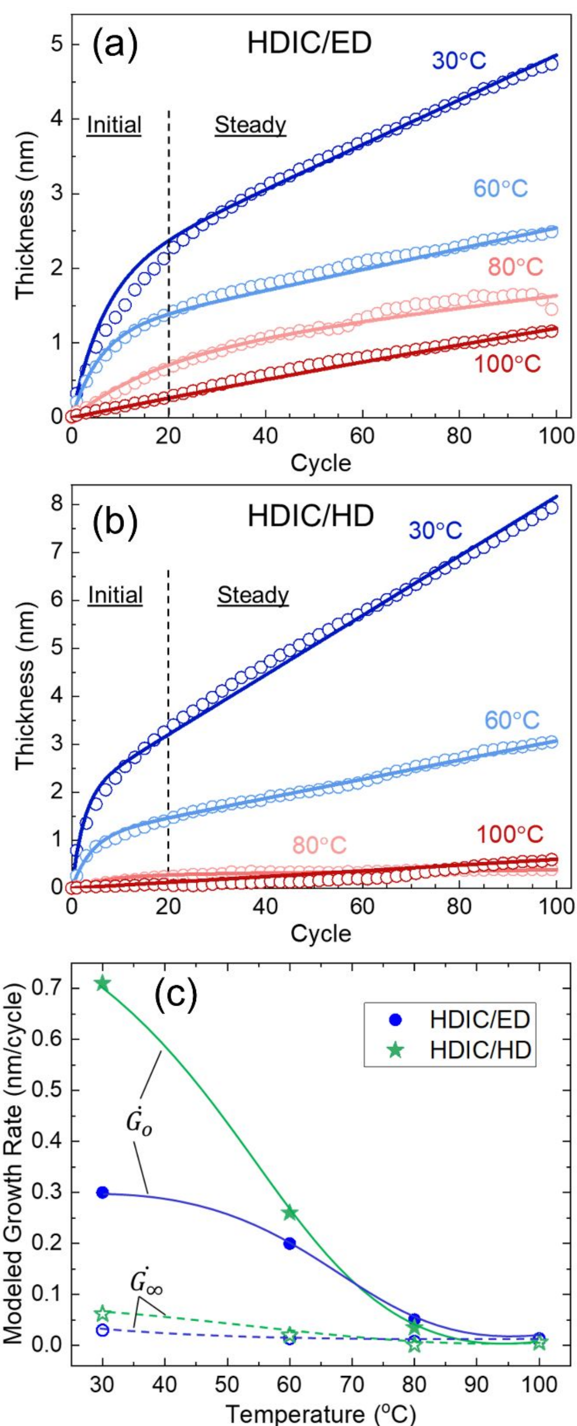

Fig. 9 Thickness versus cycle from in situ ellipsometry measurements for (a) HDIC/ED and (b) HDIC/HD deposited at 30 (dark blue), 60 (light blue), 80 (light red), and 100 °C (dark red) on hydroxylated SiO_2 substrates. Lines correspond to model fit presented in Table 2. (c) Summary of $\dot{G}_\infty$ (open shapes, dashed lines) and $\dot{G}_o$ (solid shapes, solid lines) from model for HDIC/ED (blue) and HDIC/HD (green). Trends in panel (c) are guides to the eye

This journal is © The Royal Society of Chemistry 20xx

Please do not adjust margins

Discussion

The ellipsometry and QCM data presented above show that under steady growth conditions, the polyurea growth rate depends on monomer structure (aromatic vs aliphatic), monomer size (2-carbon vs 6-carbon chains), and substrate temperature. Moreover, we find that for each polymer type, the growth rate changes during the first ~20 cycles of growth, where the extent of change depends on the monomer, temperature, and substrate material (metal oxide vs aromatic vs aliphatic).

Generally, the addition of a monomer to a growing surface occurs via reaction at a reactive site on the exposed substrate.[28,35] Under near-saturation conditions, the extent of film growth is expected to be proportional to the density of active sites per unit area available on the surface. Therefore, we can understand the observed trends in film growth in terms of the change in active site density as the growth proceeds. For any polymer deposition, the number of available sites can be influenced by three mechanisms: 1) a steric effect, where the incoming monomer initially reacts at one surface site to create a new site for the next half-cycle, but blocks other adjacent active sites;[9,63] 2) the incoming monomer reacts at multiple sites that are close to each other (i.e., a double reaction, DR)[28,34] which consumes sites and creates no new sites for the next half-cycle;[28,34] and 3) precursor adsorption and sub-surface diffusion, where precursors physisorb and create active sites for the next half-cycle without consuming any active sites.[28] These mechanisms are expected to be influenced by the reactant size and mechanical properties. Therefore, the reactant sets studied here with different monomer lengths and flexibilities, PDIC/ED (stiff, short), PDIC/HD (stiff, long), HDIC/ED (flexible, short), and HDIC/HD (flexible, long), can give insight into trends in the reaction mechanisms.

Considering the initial growth rate ($\dot{G}_o$) on metal oxide substrates, results in Figures 7, 9, and 10 show that both the aromatic and aliphatic polyurea start depositing at a high rate, followed by a decrease to a steady value. The initially higher rate is ascribed to a relatively larger density of active sites (i.e., hydroxyl groups) on the starting Si-OH or Al-OH surfaces compared to that (i.e., –N=C=O or $–NH_2$ groups) on the growing polyurea. The initial growth rate for the aromatic PDIC is larger than the rate using HDIC, suggesting that the more flexible HDIC promotes more DRs, even during the first deposition cycles.[35]

The steady growth rate ($\dot{G}_\infty$), also depends on the MLD reactants. As shown in Table 2, polymers containing the more rigid aromatic PDIC have larger $\dot{G}_\infty$ than those with the more flexible HDIC, consistent with more DRs for the more flexible reactants. Also using the PDIC, the shorter ED co-reactant gives a larger growth rate than the longer HD, suggesting the longer molecule favors more DRs. However, using the HDIC, the longer HD shows a larger growth rate than the shorter ED. Because DRs require two sites that are close together, DRs are less likely when the growth rate is small, i.e. when there are few active sites on the surface. Therefore, the larger growth rate for HDIC/HD compared to HDIC/ED may be related to the larger size and/or larger adsorptivity of the HD reactant.

We can also consider how the precursors influence the fractional change in growth rate from the first cycle to steady state, and the growth rate transition parameter, γ, shown in Table 2. The decrease in growth rate is generally ascribed to a decrease in active sites available for growth caused by the combined influence of steric hindrance and DR's.[28] For deposition at 60 °C on Si-OH, the more flexible HDIC monomer (for both HDIC/ED and HDIC/HD) shows >90 % decrease in growth rate, whereas the more rigid PDIC-containing films demonstrate a decrease in growth rate of only ~64 %. The larger fractional change in growth rate for the more flexible polymers is likely due to more prevalent DRs.

Table 2 Summary of experimental growth rates, change in growth rate, and model fitting parameters for each polymer film deposited on hydroxylated SiO_2 at various temperatures. Experimental steady growth rates were calculated by taking the average growth rate from cycle 30 to 100.

Polymer	Deposition Temperature (°C)	Experiment		Model				Figure
		$\dot{G}_o$ (nm/cycle)	$\dot{G}_\infty$ (nm/cycle)	$\dot{G}_o$ (nm/cycle)	$\dot{G}_\infty$ (nm/cycle)	Fractional Change	γ	
PDIC/ED	60	0.91	0.33	0.91	0.33	64%	2.4	7, 10
PDIC/HD	45	0.27	0.12	0.27	0.10	63%	3.7	7
HDIC/ED	30	0.32	0.029	0.30	0.030	90%	6.5	9
	60	0.21	0.013	0.20	0.014	93%	5.8	7, 9, 10
	80	0.078	0.0079	0.051	0.008	84%	19	9
	100	0.014	0.011	0.014	0.011	21%	60	9
HDIC/HD	30	0.78	0.057	0.71	0.062	91%	2.5	9
	60	0.26	0.020	0.26	0.020	92%	4.0	7, 9
	80	0.033	0.0014	0.035	0.0011	97%	7.5	9
	100	0.0071	0.0073	0.0071	0.0060	16%		9

Please do not adjust margins

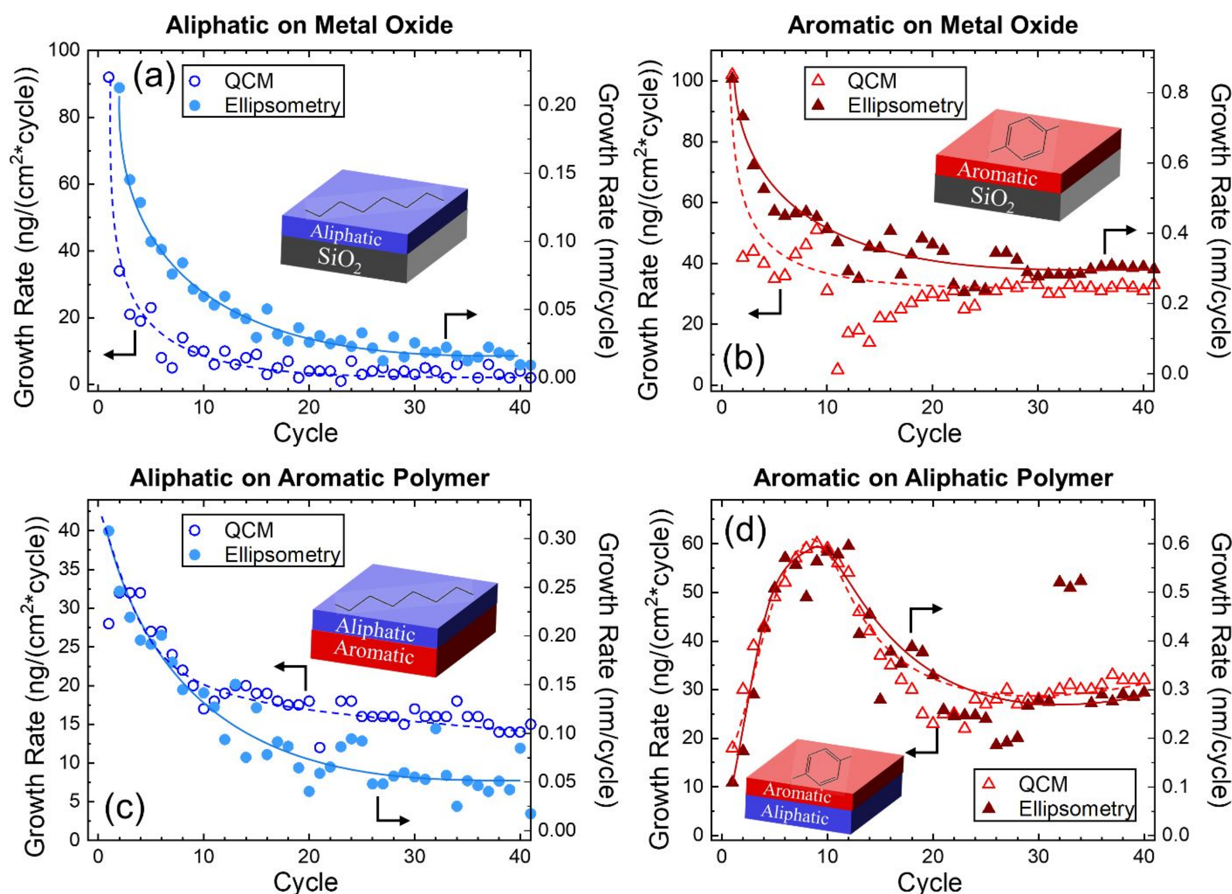

Fig. 10 Growth rate versus cycle at 60°C from in situ ellipsometry (solid shapes, right y-axis) and QCM (open shapes, left y-axis) data for (a) aliphatic polyurea (HDIC/ED, blue) on metal oxide, (b) aromatic polyurea (PDIC/ED, red) on metal oxide, (c) aliphatic polyurea on aromatic polymer, and (d) aromatic polyurea on aliphatic polymer. Lines are drawn as guides to the eye.

The values of the transition parameter also show interesting trends for the different polymers. For deposition at 60 °C, the data in Table 2 shows that the value for γ varies inversely with steady growth rate (i.e., $\gamma_{PDIC/ED} < \gamma_{PDIC/HD} < \gamma_{HDIC/HD} < \gamma_{HDIC/ED}$). Interestingly, for the data in Table 2, we find that the film thickness at which the transition in growth rate occurs (i.e. film thickness when n = γ) is 1.1 ± 0.4 nm for each polymer. Thus, the transition from initial to steady growth occurs at about the same film thickness for each film.

In addition, the inverse relation between γ and steady growth rate is also maintained for the data in Figure 9 for HDIC/ED and HDIC/HD deposited at different temperatures. Between 30 and 100 °C, the density of –OH sites on the hydroxylated SiO_2 surface is expected to not depend on temperature,[64] but the extent of physisorption is expected to decrease strongly with increasing temperature.[57] While more data and analysis is needed to fully understand the observed growth rate transitions, it is reasonable to expect that fewer physisorption reactions promote a more rapid transition to steady growth.

On the polymer substrates (Fig. 10), aliphatic HDIC/ED growth on aromatic PDIC/ED shows a similar trend for the growth rate compared to that on SiO_2, whereas aromatic growth on the aliphatic substrate shows a more complex trend. The small initial growth rate is consistent with the small density of growth sites on the slower-growing HDIC/ED substrate surface. The subsequent increase in growth rate (i.e. increase in reactive sites) is likely due to physisorption, with few DRs due to the low density of sites. As growth proceeds, DRs start to become prominent, decreasing the growth rate (i.e. decrease in reactive sites) until a balance is obtained at the steady growth rate. Evidence for more favorable physisorption on the growing aliphatic surface is present in the FTIR results in Fig. 6, where the decreased amide peak splitting indicates stronger hydrogen-bonding in the aliphatic films compared to the aromatic structures.[9,35] The growth rate "inertia" apparent in the transition from lower initial growth to higher steady growth is likely due to differences in the relative cycle number at which DRs increase in frequency and physisorption decreases in frequency. For example, if more cycles are required for DRs to become significant compared to when physisorption becomes significant, then we would expect to see the trend observed in Figure 10d. Previous studies[28,59,65] have also demonstrated this growth rate "inertia", where an increasing growth rate reaches a value higher than the expected steady value before decreasing back to the steady rate. Further experiments are

This journal is © The Royal Society of Chemistry 20xx

required to more fully elucidate the mechanisms involved during polyurea MLD on polymer surfaces.

Conclusions

This work reports polyurea MLD using the highly flexible hexamethylene diisocyanate (HDIC) precursor, and directly compares growth to that using the more common phenylene diisocyanate (PDIC) using HD or ED as diamine co-reactants. Compared to the PDIC, the HDIC demonstrated improved thermal stability and reliable precursor delivery, even after prolonged (> 6 months) heating in the reactant vessel.

Results using in situ ellipsometry gave insight into growth evolution, showing substantial changes in film growth rate during the first ~20 MLD cycles, where the extent of change depended on reactant composition and structure, as well as starting substrate composition and substrate temperature. The transition from initial to steady growth is attributed to a change in active site density as the growth proceeds from the initial starting substrate, where the number of sites is influenced by a balance between steric effects that block active sites, double reactions that consume multiple active sites, and site creation by precursor physisorption and sub-surface diffusion. We further conclude that the extent of each of these mechanisms depends on the film thickness as well as the flexibility, length, and structure of the isocyanate and amine reactants used in the MLD sequence. The mechanistic insight described here will provide a basis for more advanced modeling to better understand the detailed complexity of reactions during deposition of ultra-thin organic thin films for advanced electronic and other applications.

Conflicts of interest

There are no conflicts to declare.

Acknowledgements

This material is based upon work supported by the US Department of Defense Multidisciplinary Research Program of the University Research Initiative, under Grant No. W911NF-16-1-0406. The authors acknowledge the access to the Analytical Instrumentation Facility (AIF) at North Carolina State University, supported by the State of North Carolina and National Science Foundation.

References

1 S. H. Cha, A. Park, K. H. Lee, S. Im, B. H. Lee and M. M. Sung, *Org. Electron.*, 2010, **11**, 159–163.

2 Y.-S. Park, S.-E. Choi, H. Kim and J. S. Lee, *ACS Appl. Mater. Interfaces*, 2016, **8**, 11788–11795.

3 X. Li, A. Lushington, Q. Sun, W. Xiao, J. Liu, B. Wang, Y. Ye, K. Nie, Y. Hu, Q. Xiao, R. Li, J. Guo, T.-K. Sham and X. Sun, *Nano Lett.*, 2016, **16**, 3545–3549.

4 C. MacIsaac, J. R. Schneider, R. G. Closser, T. R. Hellstern, D. S. Bergsman, J. Park, Y. Liu, R. Sinclair and S. F. Bent, *Adv. Funct. Mater.*, 2018, **28**, 1800852.

5 D. H. Kim, S. E. Atanasov, P. Lemaire, K. Lee and G. N. Parsons, *ACS Appl. Mater. Interfaces*, 2015, **7**, 3866–3870.

6 S. E. Atanasov, M. D. Losego, B. Gong, E. Sachet, J.-P. Maria, P. S. Williams and G. N. Parsons, *Chem. Mater*, 2014, **26**, 3471–3478.

7 S. Lehtimä, M. Suominen, P. Damlin, S. Tuukkanen, C. Kvarnströ and D. Lupo, *ACS Appl. Mater. Interfaces*, 2015, **7**, 22137–22147.

8 L. Momtazi, D. A. Dartt, O. Nilsen and J. R. Eidet, *J. Biomed. Mater. Res. Part A*, 2018, **106**, 3090–3098.

9 A. Lushington, C. Langford, J. Liu, K. Nie, R. Li, X. Sun, J. Guo and X. Sun, *J. Phys. Chem. C*, 2017, **121**, 11757–11764.

10 B. H. Lee, K. R. Min, S. Y. Choi, K. H. Lee, S. Im and M. M. Sung, *J. Am. Chem. Soc.*, 2007, **129**, 16034–16041.

11 A. I. Abdulagatov, K. E. Terauds, J. J. Travis, A. S. Cavanagh, R. Raj and S. M. George, *J. Phys. Chem. C*, 2013, **117**, 17442–17450.

12 A. Lushington, J. Liu, M. N. Bannis, B. Xiao, S. Lawes, R. Li and X. Sun, *Appl. Surf. Sci.*, 2015, **357**, 1319–1324.

13 J. Liu, B. Yoon, E. Kuhlmann, M. Tian, J. Zhu, S. M. George, Y. C. Lee and R. Yang, *Nano Lett.*, 2013, **13**, 5594–5599.

14 B. H. Lee, B. Yoon, V. R. Anderson and S. M. George, *J. Phys. Chem. C*, 2012, **116**, 3250–3257.

15 D. C. Miller, R. R. Foster, Y. Zhang, S.-H. Jen, J. A. Bertrand, Z. Lu, D. Seghete, J. L. O'patchen, R. Yang, Y.-C. Lee, S. M. George and M. L. Dunn, *J. Appl. Phys*, 2009, **105**, 93527.

16 C. Y. Kao, B. Li, Y. Lu, J. W. Yoo and A. J. Epstein, *J. Mater. Chem. C*, 2014, **2**, 6171–6176.

17 L. Yan, X. Wang, S. Zhao, Y. Li, Z. Gao, B. Zhang, M. Cao and Y. Qin, *ACS Appl. Mater. Interfaces*, 2017, **9**, 28.

18 B. Cardineau, R. Del Re, M. Marnell, H. Al-Mashat, M. Vockenhuber, Y. Ekinci, C. Sarma, D. A. Freedman and R. L. Brainard, *Microelectron. Eng.*, 2014, **127**, 44–50.

19 H. Zhou and S. F. Bent, *ACS Appl. Mater. Interfaces*, 2011, **3**, 505–511.

20 X. Meng, *J. Mater. Chem. A*, 2017, **5**, 18326–18378.

21 X. Liang, B. W. Evanko, A. Izar, D. M. King, Y. B. Jiang and A. W. Weimer, *Microporous Mesoporous Mater.*, 2013, **168**, 178–182.

22 C. Chen, P. Li, G. Wang, Y. Yu, F. Duan, C. Chen, W. Song, Y. Qin and M. Knez, *Angew. Chemie Int. Ed.*, 2013, **52**, 9196–9200.

23 A. J. Cruz, I. Stassen, M. Krishtab, K. Marcoen, T. Stassin, S. Rodríguez-Hermida, J. Teyssandier, S. Pletincx, R. Verbeke, V. Rubio-Giménez, S. Tatay, C. Martí-Gastaldo, J. Meersschaut, P. M. Vereecken, S. De Feyter, T. Hauffman, R. Ameloot, C. Marti-Gastaldo, J. Meersschaut, P. M. Vereecken, S. De Feyter, T. Hauffman, R. Ameloot, C. Martí-Gastaldo, J. Meersschaut, P. M. Vereecken, S. De Feyter, T. Hauffman and R. Ameloot, *Chem. Mater.*, 2019, **31**, 9462–9471.

24 H. F. Barton, A. K. Davis and G. N. Parsons, *ACS Appl. Mater. Interfaces*, 2020, 12, 14690–14701.

25 A. J. Cruz, G. Arnauts, M. Obst, D. E. Kravchenko, P. M.

Vereecken, S. De Feyter, I. Stassen, T. Hauffman and R. Ameloot, *Dalt. Trans.*, 2021, **50**, 6784–6788.
26 H. Zhou, M. F. Toney and S. F. Bent, 2013, **46**, 5643.
27 B. Yoon, D. Seghete, A. S. Cavanagh and S. M. George, *Chem. Mater*, 2009, **21**, 5365–5374.
28 D. S. Bergsman, R. G. Closser and S. F. Bent, *Chem. Mater.*, 2018, **30**, 5087–5097.
29 K. Van De Kerckhove, F. Mattelaer, D. Deduytsche, P. M. Vereecken, J. Dendooven and C. Detavernier, *Dalt. Trans.*, 2016, **45**, 1176–1184.
30 Y. H. Li, D. Wang and J. M. Buriak, *Langmuir*, 2010, **26**, 1232–1238.
31 D. Seghete, R. A. Hall, B. Yoon and S. M. George, *Langmuir*, 2010, **26**, 19045–19051.
32 G. N. Parsons, S. E. Atanasov, E. C. Dandley, C. K. Devine, B. Gong, J. S. Jur, K. Lee, C. J. Oldham, Q. Peng, J. C. Spagnola and P. S. Williams, *Coord. Chem. Rev.*, 2013, **257**, 3323–3331.
33 A. H. Brozena, C. J. Oldham and G. N. Parsons, *J. Vac. Sci. Technol. A*, 2016, **34**, 010801.
34 R. A. Nye, A. P. Kelliher, J. T. Gaskins, P. E. Hopkins and G. N. Parsons, *Chem. Mater.*, 2020, **32**, 1553–1563.
35 D. S. Bergsman, R. G. Closser, C. J. Tassone, B. M. Clemens, D. Nordlund and S. F. Bent, *Chem. Mater.*, 2017, **29**, 1192–1203.
36 K. Che, P. Lyu, F. Wan and M. Ma, *Materials (Basel).*, 2019, **12**, 3636.
37 A. Kim, M. A. Filler, S. Kim and S. F. Bent, *J. Am. Chem. Soc*, 2005, **127**, 6123–6132.
38 R. G. Closser, D. S. Bergsman, L. Ruelas, F. S. M. Hashemi and S. F. Bent, *J. Vac. Sci. Technol. A Vacuum, Surfaces, Film.*, 2017, **35**, 031509.
39 U.-J. Choi, H. Kim, Y.-S. Park and J. S. Lee, *Bull. Korean Chem. Soc.*, 2018, **39**, 119–122.
40 J. S. Lee, Y.-J. Lee, E. L. Tae, Y. S. Park and K. B. Yoon, *Science (80-.).*, 2003, **301**, 818–821.
41 Y. Chen, B. Zhang, Z. Gao, C. Chen, S. Zhao and Y. Qin, *Carbon N. Y.*, 2015, **82**, 470–478.
42 PubChem Compound Summary for CID 61009, 1,4-Phenylene diisocyanate.
43 PubChem Compound Summary for CID 13192, Hexamethylene diisocyanate., https://pubchem.ncbi.nlm.nih.gov/compound/13192#section=ICSC-Number, (accessed 11 August 2021).
44 PubChem Compound Summary for CID 16402, 1,6-Hexanediamine., https://pubchem.ncbi.nlm.nih.gov/compound/1_6-Hexanediamine#section=Computed-Properties, (accessed 11 August 2021).
45 PubChem Compound Summary for CID 3301, Ethylenediamine, https://pubchem.ncbi.nlm.nih.gov/compound/Ethylenediamine, (accessed 11 August 2021).
46 R. Richter, H. Ulrich and D. J. Duchamp, *J. Org. Chem.*, 1978, 43, 3060–3063.
47 R. E. Buckles and L. A. McGrew, *J. Am. Chem. Soc*, 1963, **335**, 185.
48 R. G. Arnold, J. A. Nelson and J. J. Verbanc, *Chem. Rev.*, 1956, **57**, 47–76.
49 S. Dabi and A. Zilkha, *Eur. Polym. J.*, 1980, **16**, 831–833.
50 H. Jain and P. Poodt, *Dalt. Trans.*, 2021, **50**, 5807–5818.
51 E. Langereis, S. B. S. Heil, H. C. M. Knoops, W. Keuning, M. C. M. van de Sanden and W. M. M. Kessels, *J. Phys. D. Appl. Phys.*, 2009, **42**, 073001.
52 N. M. Adamczyk, A. A. Dameron and S. M. George, *Langmuir*, 2008, **24**, 2081–2089.
53 P. W. Loscutoff, H. Zhou, S. B. Clendenning and S. F. Bent, *ACS Nano*, 2010, **4**, 331–341.
54 M. M. Coleman, M. Sobkowiak, G. J. Pehlert, P. C. Painter and T. Iqbal, *Macromol. Chem. Phys.*, 1997, **198**, 117–136.
55 J. Joseph and E. D. Jemmis, *J. Am. Chem. Soc.*, 2007, **129**, 4620–4632.
56 M. Putkonen, J. Harjuoja, T. Sajavaara and L. Niinistö, *J. Mater. Chem.*, 2007, **17**, 664–669.
57 S. M. George, B. Yoon and A. A. Dameron, *Acc. Chem. Res.*, 2009, **42**, 498–508.
58 Y. Du and S. M. George, *J. Phys. Chem. C*, 2007, **111**, 8509–8517.
59 G. N. Parsons, *J. Vac. Sci. Technol. A*, 2019, **37**, 020911.
60 C. Zhang, M. Vehkamäki, M. Pietikäinen, M. Leskelä and M. Ritala, *Chem. Mater.*, 2020, **32**, 5073–5083.
61 J.-W. J. Clerix, E. A. Marques, J. Soethoudt, F. Grillo, G. Pourtois, J. R. Van Ommen and A. Delabie, *Adv. Mater. Interfaces*, 2021, **8**, 2100846.
62 J.-S. Kim and G. N. Parsons, *Chem. Mater.*, 2021, acs.chemmater.1c02842.
63 S. Kim, S. Lee, S. Y. Ham, D. H. Ko, S. Shin, Z. Jin and Y. S. Min, *Appl. Surf. Sci.*, 2019, **469**, 804–810.
64 S. E. Atanasov, B. Kalanyan and G. N. Parsons, *J. Vac. Sci. Technol. A Vacuum, Surfaces, Film.*, 2016, **34**, 01A148.
65 E. Stevens, Y. Tomczak, B. T. Chan, A. Sanchez, G. N. Parsons, A. Delabie and K. Leuven, *Chem. Mater.*, 2018, **3D**, 3223–3232.

 This journal is © The Royal Society of Chemistry 20xx

Please do not adjust margins